

Review

Ferroelastic Domain Boundary-Based Multiferroicity

Ekhard K. H. Salje^{1,2,*} and Xiangdong Ding^{1,*}

¹ State Key Laboratory for Mechanical Behavior of Materials, Xi'an Jiao Tong University, Xi'an 710049, China

² Department of Earth Sciences, Cambridge University, Cambridge CB2 3EQ, UK

* Correspondence: ekhard@esc.cam.ac.uk (E.K.H.S.); dingxd@mail.xjtu.edu.cn (X.D.);

Tel.: +44-1223-333400 (E.K.H.S.); +86-29-82668610 (X.D.);

Fax: +44-1223-333450 (E.K.H.S.); +86-29-82663453 (X.D.)

Academic Editor: Helmut Cölfen

Received: 16 September 2016; Accepted: 3 December 2016; Published: 9 December 2016

Abstract: Domain boundary engineering endeavors to develop materials that contain localized functionalities inside domain walls, which do not exist in the bulk. Here we review multiferroic devices that are based on ferroelectricity inside ferroelastic domain boundaries. The discovery of polarity in CaTiO_3 and SrTiO_3 leads to new directions to produce complex domain patterns as templates for ferroic devices.

Keywords: domain boundary engineering; domain walls; vortex; Bloch lines; tweed

1. Introduction

Arguably, the greatest progress in ferroic device designs during the last decade is related to the idea that the ferroic (or transport/conductivity) properties are related to interfaces and surfaces and not to the bulk. This means that high memory capacities and electrical wiring on a much finer scale than achievable with bulk technologies may be possible when only domain boundaries contain the desired functionalities [1–15]. This is not only the case for ferroelectricity or ferromagnetism, but also for electrical conductivity. Domain boundaries were already found to carry high currents, and it was the discovery of superconducting twin boundaries [16] that opened a wide field of applications in “domain boundary engineering”, where the domain boundary is the device and where the design of the device materials depends largely on tailoring appropriate domain boundaries [4,5]. Furthermore, electric dipole moments were observed inside ferroelastic domain walls so that switchable ferroelectricity is potentially confined to domain walls and cannot interfere with depolarization fields and additional switching of domains in the bulk. The length scale of the active device is then restricted to the size of domain walls or to even smaller features, such as Bloch walls, inside domain walls [16–22]. For many applications, the aim is to produce high wall concentrations. The highest concentration of “domain boundaries” was predicted for a tweed structure, which is a densely interwoven network of domain walls [23–28]. Tweed has another property: it can form a domain glass with a nonergodic response to external forcing. Domain glass [29,30] can contain polar nanoregions, which are known to exist in relaxor materials [31–34]. Complex domain structures, including tweed, may be stabilized by defects, while dynamic tweed [26] exists also for very low defect concentrations [35]. It was then argued that tweed structures are polar, either via the flexoelectric effect or via bilinear coupling between the strain and local dipole moments [36–41]. Recently, Salje et al. [42] reported the first experimental evidence for piezoelectricity of a tweed structure in LaAlO_3 , where the uniform parent structure is centrosymmetric and shows no bulk polarity.

Nanoscale-generated (multi-) ferroic materials are different from bulk ferroics, which are a well-known class of anisotropic, nonlinear solids that develop a spontaneous order parameter, usually passing through a symmetry-lowering transition point. Ferroics are classified according to their primary

order parameters, which include strain ϵ (ferroelastic), polarization P (ferroelectric), and magnetization M (ferromagnetic), where the term “ferro” designates the uniform alignment of the spontaneous moments in neighboring unit cells. Ferri- and antiferro-phases exist when the order parameter is locally rotated against a crystallographic axis, or when the relevant wavevector (or wavevectors) associated with the structural instability occur(s) at special points at the surface of the Brillouin zone. Incommensurate phase transitions require a complex order parameter with a repetition unit that is not commensurate with the underlying crystal structure. In both of these cases, the translation invariance of the order parameter (incommensurate or commensurate) is preserved throughout the crystal. There are classic textbooks on ferroics [43–54], and numerous recent reviews and research articles on multiferroics [4,5,29,55–59]. Incommensurate phases represent a borderline between the bulk ferroic behavior and the ferroicity of the modulation, and they may represent a new class of ferroic materials that have not yet been explored [60].

Unlike nanoscale-generated multiferroics, domain boundary based ferroics are equivalent to bulk ferroics in lower dimensional subspaces (as predicted by symmetry arguments by Janovec and collaborators [61–65]), such as two-dimensional twin boundaries, and one-dimensional Bloch lines and vortex dots. These subspaces are mostly defined by another bulk ferroic property, namely the ferroelastic twin patterns. Bulk ferroelasticity generates the twin walls which then can become ferroelectric, superconducting, magnetic, and so forth. Only these latter properties are used in the anticipated device applications.

Much research has been dedicated to surfaces, but any practical applications are unlikely to be confined to surfaces because the total number of particles involved in functionalities will simply be too small (unless the grain size becomes very small). This problem can be overcome when we consider parallel twin boundaries where the number of atoms inside the twin boundaries is much larger than in surface layers. From the Kittel formula for ultrathin films [4], concentrations that are much larger than 4% of the domain wall material can be estimated, and, indeed, twin domains as small as 5 nm have been observed in TbMnO_3 [66], suggesting that the number of atoms inside twin walls can be close to 50%. Meanwhile, in ferroelectric superlattices, Yadav et al. [67] have reported similarly small domains, showing also that the walls between these domains are fully chiral, forming vortices. This is an important result, as it not only shows that the fraction of domain wall material can be very large, but also shows the association between walls and chirality. This concentration is large enough to anticipate applications such as memory devices, heat regulators, and elastic dampers [59]. In addition, templates such as twin boundaries are mobile under fields and can form dynamic tweed and domain glasses [29,30]. One may then ask: Is it possible to arrange twin boundaries topologically in ways so that the macroscopic use of the material as conductors, switches, or heat regulators can be optimized? The answer is affirmative and leads to the development of domain structures, with a high degree of complexity [65–69]. This does not mean, however, that all domain walls, which are symmetry-allowed to display ferroic properties, do so in a measurable way. Careful measurements have shown that many materials with very high densities of domain walls and highly complex nanostructures did not show multiferroic properties [70–75] although they were counted as archetypal candidates for ferroelectricity. We now describe specific cases where ferroic domain boundaries were proven to exist.

2. CaTiO_3

The first example for a polar domain wall was found in CaTiO_3 [17,19,20]. As shown in Figure 1, two lines of research came together in this material. First, it was shown that twin and antiphase boundaries represent sinks for oxygen vacancies. The stabilization energy for oxygen vacancies was predicted to be ca. 0.7 eV with a repulsive interaction between vacancies [76–79]. It is expected, therefore, that oxygen vacancies are rather uniformly distributed within twin walls and depleted in the bulk [78]. The second prediction is based on the inherent instability of regular TiO_6 octahedra. Even an oxygen cage with cubic symmetry and of sufficient size will lead to off-centering of the Ti position so that it is probable that distorted octahedra will contain Ti located slightly off the

geometrical midpoint of the octahedra [20]. Such geometrical configurations contain electric dipole moments, which, depending on the nature of the dipole–dipole interaction, will lead to ferroelectric or ferrielectric local centers. Numerical calculations have shown that domain boundaries in CaTiO_3 are mainly ferrielectric with maximum dipole moments at the wall [20]; a small ferroelectric dipole moment was found perpendicular to the wall with alternating (antiferroelectric) dipoles between neighboring walls. The same tendency for polar layers in CaTiO_3 (e.g., near surfaces) was also predicted for $\text{CaTiO}_3/\text{BaTiO}_3$ interfaces [80]. In CaTiO_3 the resulting polarity of the domain wall was observed by high-resolution transmission electron microscopy [17], which represented the first proof that such wall-related polar structures exist in ferroelastic materials.

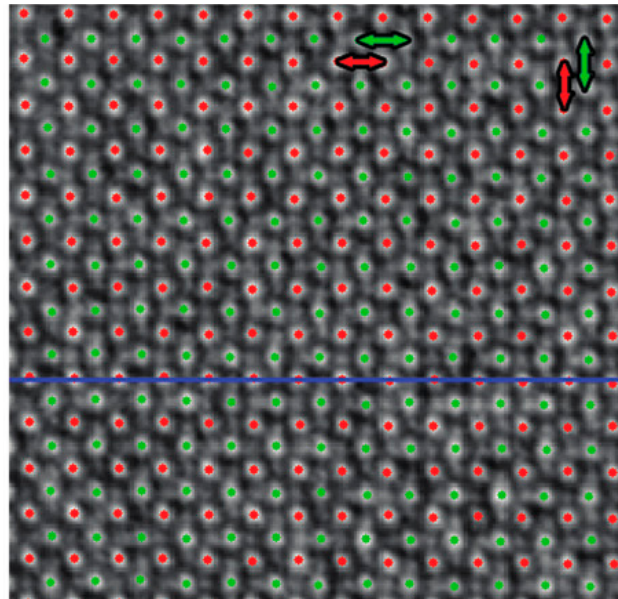


Figure 1. Image of a twin wall in CaTiO_3 with polar shifts of Ti positions inside the wall and two adjacent layers of Ti shifts towards the wall center [17].

Details of the symmetry of the polar vector were subsequently determined by Yokota et al. [19] using second harmonic generation (SHG) techniques. Three-dimensional SHG images of samples with the pseudocubic (110) and (1–11) planes confirmed that both crystallographically prominent types of twin boundaries (W plane) and nonprominent twin boundaries (W' plane) are SHG active and, consequently, polar. The directions of the electric polarization P were determined from the anisotropy of SHG intensities. In the W' plane, the SHG polar diagrams are well fitted using the point-group symmetry 2, which reveals that the P directions are parallel to the twofold axis. They do not lie in the W' plane, but are tilted from it. In the W plane, the P direction lies in the mirror plane of the point-group symmetry m . These studies are probably the most precise SHG investigations ever undertaken in domain boundary engineering and demonstrate the power of this technique. The resonant piezoelectric effect in CaTiO_3 was recently reported by Salje et al. [81].

3. SrTiO_3

SrTiO_3 is an incipient ferroelectric, so it is not surprising that ferroic properties emerge near defects, surfaces, and domain boundaries [82]. This is in contrast to CaTiO_3 , which is not an incipient ferroelectric, although the detailed mechanisms of the off-centering of Ti in SrTiO_3 and CaTiO_3 are almost identical. Energy minimization of empirical potentials [18] show reduced tilts of the TiO_6 octahedra (Figure 2) near the twin boundary and, again in contrast with CaTiO_3 , a shift of both cations, namely Ti and Sr (Figure 3) from the center of symmetry. The polar properties are still dominated by Ti with the underlying ferroelastic twin structures being extremely sensitive to external forces.

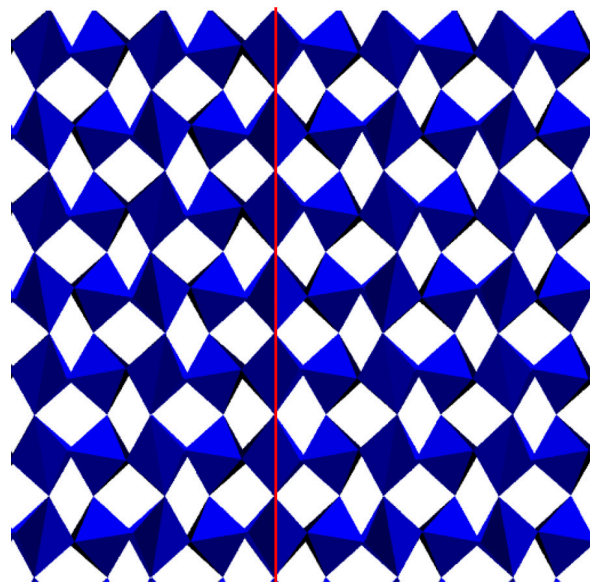


Figure 2. A snapshot of the TiO_6 octahedral tilts in the vicinity of the twin wall (vertical red line). Notice the change of the tilting angles across the boundary [18].

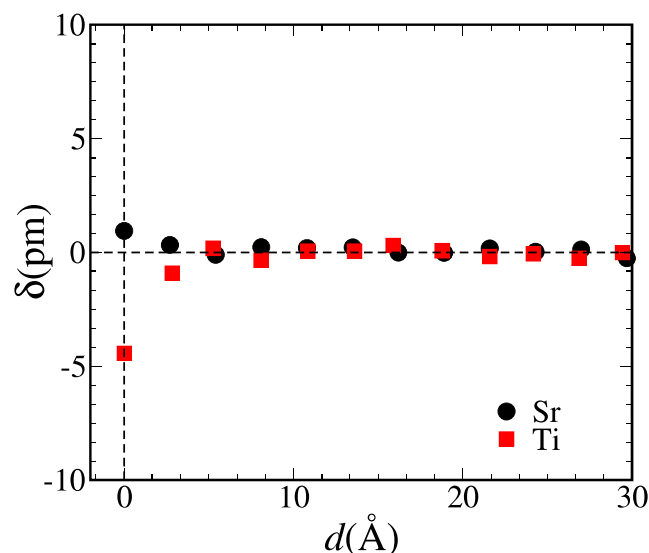


Figure 3. The variation of the Sr–Sr and Ti–Ti nearest-neighbor distances in the bulk and near the twin wall against the distance perpendicular to the wall [18].

The great mobility of twin walls in SrTiO_3 was documented by Kityk et al. [83,84], and the high density of twin walls and dislocations near the crystal surface was shown by X-ray diffraction [85] and optical microscopy [86]. Wall polarity was observed by resonant piezoelectric spectroscopy (RPS) [13,21] at temperatures well below the ferroelastic phase transition [87]. Fontcuberta et al. [88] have shown that electric tuning of ferroelastic domain walls in SrTiO_3 also leads to dramatic changes of the magnetic domain structure of a neighboring magnetic layer ($\text{La}_{1/2}\text{Sr}_{1/2}\text{MnO}_3$) epitaxially clamped on a SrTiO_3 substrate. They showed that the properties of the magnetic layer are intimately connected to the existence of polar regions at twin boundaries of SrTiO_3 that can be electrically modulated. These findings illustrate that by exploiting the responsiveness of domain walls (DWs) to external stimuli—even in absence of any domain contribution—prominent and adjustable macroscopic reactions of neighboring layers can be obtained. Domain walls can hence be used to trigger tunable magnetic responses and may lead to new ways for the manipulation of emerging multiferroic properties.

The new aspect of polarity inside domain walls in SrTiO₃ relates to the high degree of isotropy of this weakly distorted structure. While in CaTiO₃ the direction of the electric dipole is always oriented towards the apex of the twin structure, all indications in SrTiO₃ are that the energy required to reverse the dipole is small and comparable with the thermal energy. This means that dipole configurations such as that shown in Figure 4 are rather common. An indirect proof for such polar structures stems from the observation of resonance structures at cryogenic temperatures [13], which coincide with the results of simulations [18].

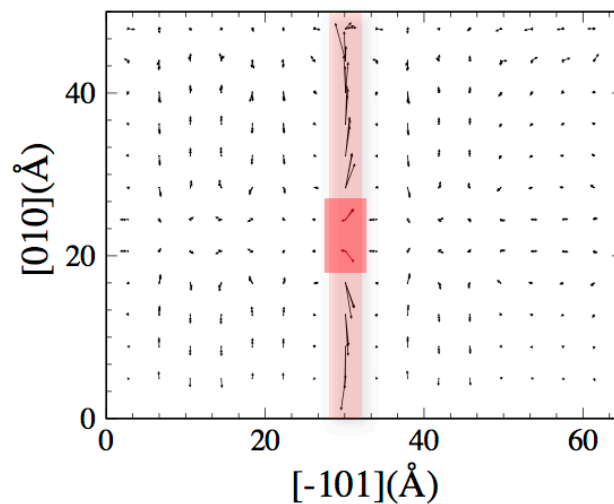


Figure 4. Vortex structure of Ti-displacements at an inversion point inside a twin wall in SrTiO₃ [18]. The view is perpendicular to the twin wall, which is pointing inside the plane of view. All Ti-displacements from the octahedral midpoints are small inside the two adjacent domains, but large inside the pink domain wall. The rotation of the displacement vectors inside the domain wall constitutes a Bloch wall [22] and is indicated in red.

These local reversals constitute local vortex structures, where the dipole rotates out of the twin plane and have been investigated in [89,90]. RPS studies in [21] evidenced field-induced deformations, which were attributed to local piezoelectricity inside domain walls.

Theoretical arguments lead to the conclusion that vortex structures are expected to exist [68,69] although no direct domain observations were yet reported. Nevertheless, the results of Zhao et al. [69] were directly inspired by the simulations in SrTiO₃ [18] and may yet be the strongest evidence that such flicker vortex states may be observable in SrTiO₃. Despite the short lifetime of each vortex, these authors reported that the vortex density of the sample remains constant and can be modulated with weak electric fields. It is the local instability of the vortex state that makes it possible to switch vortices locally and also change the global vortex density. These bulk effects are mirrored by domain wall vortices, even if these vortices do not exist in the bulk. The first clear indication of this effect came from molecular dynamics studies [18,69,85,91]. It was shown that the orientation of the polar vectors in the wall could invert if the anisotropy energy is sufficiently small. Simulated polar patterns in the domain walls with rotations of the dipoles out of the wall are shown in Figure 4. The rotation leads to Bloch-like states in the wall, where the dipole is oriented perpendicular to the wall (Figure 5). Interestingly, this result is almost identical to analytical predictions [39,92].

Usually, polarity in twin walls is ferrielectric, whereas vortex excitations lead to true ferroelectricity on a very local scale. As a result, in-plane electric fields can selectively stabilize one of the vortex polarization states and enhance the ability of the walls to move. For nanoscale ferroelectric memory devices, one envisages a precisely controllable device, where a desired domain wall pattern is manipulated by shifting the vortex position electrically or mechanically. Molecular dynamics simulations mimic this situation, where a constant electric field acts as an external force individually

applied to the charged atoms or dipoles along the direction of the field. To characterize the local response of the vortex polarization to the field, Zykova-Timan and Salje tuned the initial experimental input to the specifications of the atomistic model (e.g., dielectric permittivity of SrTiO_3 , system size, etc.). The application of high electric fields above $0.007 \text{ V}/\text{\AA}$ along $[-101]$ induced a rotation of the Ti-dipoles near the twin boundary and in the bulk structure. Thus, the vortex deformed and became unstable. In the range from -0.004 to $0.004 \text{ V}/\text{\AA}$, the twin boundary stabilized and a spontaneous switchable polarization of the vortex, aligned with the field, dominated over the initial state [81].

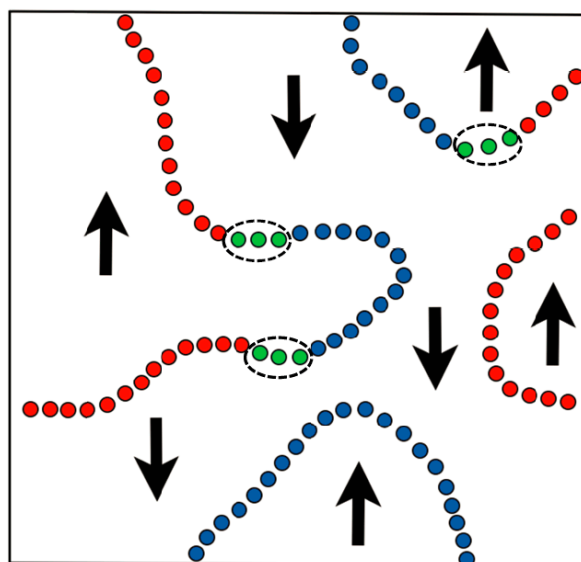


Figure 5. Twin plane with local dipole moments in the up and down direction. Bloch lines limit the domains within the twin wall where the dipole direction is either out of the plane (red) or into the plane (blue). Bloch vortex points, where two Bloch lines with different polarity join, are indicated in green [22].

We show Bloch lines inside the twin plane (-101) in Figure 5 and mark the two possible dipole directions in $[-101]$ as red and along $[10-1]$ as blue. Two switching processes can be envisaged in this geometry. The first is to apply a vertical field along the dipole direction. This field will move Bloch lines by expanding or shrinking the larger domains. The macroscopic polarization in this direction directly reflects the volume proportion of the up-and-down domains. Depending on the geometrical distribution of Bloch lines, we expect the changes of the macroscopic polarization to be continuous or abrupt (the latter happens when Bloch lines jam [41], similar to jamming of ferroelastic domains).

The second switching mechanism relates to fields perpendicular to the twin plane. In this case, there is little interaction with the dipoles in each subdomain besides some weak dipole canting. The field couples directly with the dipoles, which are orthogonal to the twin plane (red and blue in Figure 5). This may happen by switching dipoles in segments of Bloch lines into the opposite directions. This local switching does not involve the shift of Bloch points, as indicated by green segments in Figure 5, and is hence fast. Simulations of complex ferroelastic structures found switching times only slightly longer than the phonon times [93,94]. A much slower movement can be envisaged when the Bloch points shift and thereby change the ratio of red and blue domains inside the Bloch walls. This sliding of Bloch points is similar to the sliding of kink excitations in ferroelastic materials and requires ca. 50 phonon times to pass a diameter of 10 nm [95]. The total bit density of such a Bloch-line ferroelectric vertex memory can be very high [22]; we estimate that distances between twin boundaries are as small as 50 nm and that Bloch lines can form with densities of 100 Bloch lines in an area of $100 \times 100 \text{ nm}^2$, giving a bit density of $10^{16} / \text{m}^2$. This may be compared with a maximum bit density of 1.0 Tbit/sq.in. (the unusual mixed units favored in the magnetic memory industry), and it

offers potentially one order of magnitude higher density than is currently attainable. The problems of access remain; however, these can be addressed by nanolithography with e-beam writing. A separate question is one of write speed, but in the present case this is not limited by domain wall mobility, which in the low-field regime is ca. 1 nm/s [22,96,97].

4. Domain Glass and Complex Structures

Increasing the densities of domain boundaries, and hence smaller domains, leads to quantitatively new effects. The highest wall concentration was predicted for a tweed structure, which is a densely interwoven network of domain walls [23–28]. Domain glass [29,30] is vaguely akin to relaxors [31–33] although the local domain wall structures may be much better preserved. Spatially heterogeneous states like tweed depend crucially on the elastic anisotropy, while detailed stability simulations showed that tweed structures are omnipresent in any ferroelastic precursor pattern [34]. These arguments indicate that tweed is stabilized by defects while dynamic tweed also exists for very low defect concentrations [35]. It was argued that tweed structures are polar, either via the flexoelectric effect or via bilinear coupling between the strain and local dipole moments [36–38,40], although such polarity has never been observed. More generally, it was then shown that all complex ferroelastic patterns show polarity, including tweed patterns [98]. Experimentally, Salje et al. [42] reported the first direct evidence for piezoelectricity of a tweed structure in LaAlO_3 , where the uniform parent structure is centrosymmetric and shows no polarity [99].

The importance of the flexoelectric effect for the formation of such polarity in complex structures was first found by computer simulation [98]. The study of an atomistic toy model showed the interplay of ferroelastic twin patterns and electrical polarization. Molecular dynamics simulation reproduced the polarity in straight twin walls and, by making contact with continuum theory, it was demonstrated that the effect is governed by linear flexoelectricity. Complex twin patterns, with very high densities of kinks and/or junctions [100,101], produced winding structures in the dipolar field, which are reminiscent of polarization vortices. By means of a “cold shearing” technique, patches with high vortex densities were generated.

These patterns unexpectedly show a net macroscopic polarization, even if neither the original sample nor the applied mechanical perturbation breaks inversion symmetry by itself. These results explain puzzling experimental observations of “parasitic” polarity by Garten et al. [100] and Biancoli et al. [101]. It also connects with the idea that domain boundary-related multiferroic switching is not necessarily related to the switching on individual domain boundaries, but to patches of several domain boundaries [11]. This approach may become necessary because it may not be possible to address individual domain walls in a device but to cover several boundaries collectively. The memory structure would then not relate to simple binary codes (such as up or down of the polar component) but to the number of up or down of all domain boundaries in the patch. If one has, on average, 10 boundaries in a patch, one could potentially access all possible combinations between “all up” (+10) and “all down” (−10), which greatly increase the bit-density of the device.

5. Conclusions

Domain boundary engineering is an emerging field of research, which has had already great success in magnetic devices using the racetrack technology [102]. Memory devices based on ferroelectricity have not yet been developed, while the essential elements are known: namely local polarization and switchable nanostructures. Developing the device materials needs then to be accompanied by an equivalent evolution of the logical structure of the computation. It is very unlikely that binary computation will be the optimal way to use nanoscale memory device materials. Other developments, such as the memistor device, may lead to some blueprint for applications. Another previous development, such as relaxor materials for devices requiring high dielectric responses, may equally lead to some inspiration for the application of domain boundary ferroics.

Acknowledgments: We are grateful to NSFC (51320105014, 51621063) for their support. EKHS is grateful to EPSRC (EP/K009702/1) and the Leverhulme Trust (EM-2016-004).

Author Contributions: Ekhard K. H. Salje wrote the first manuscript, Xiangdong Ding and Ekhard K. H. Salje revised the paper.

Conflicts of Interest: The authors declare no conflict of interest.

References

1. Daraktchiev, M.; Catalan, G.; Scott, J.F. Landau theory of domain wall magnetoelectricity. *Phys. Rev. B* **2010**, *81*, 224118. [[CrossRef](#)]
2. Lajzerowicz, J.J.; Niez, J.J. Phase transition in a domain wall. *J. Phys. Lett.* **1979**, *40*, 165–169. [[CrossRef](#)]
3. Wojdeł, J.C.; Íñiguez, J. Ferroelectric transitions at ferroelectric domain walls found from first principles. *Phys. Rev. Lett.* **2014**, *112*, 247603. [[CrossRef](#)] [[PubMed](#)]
4. Salje, E.K.H. Multiferroic domain boundaries as active memory devices: Trajectories towards domain boundary engineering. *Chemphyschem* **2010**, *11*, 940–950. [[CrossRef](#)] [[PubMed](#)]
5. Salje, E.K.H.; Zhang, H. Domain boundary engineering. *Phase Transit.* **2009**, *82*, 452–469. [[CrossRef](#)]
6. Seidel, J.; Martin, L.W.; He, Q.; Zhan, Q.; Chu, Y.-H.; Rother, A.; Hawkridge, M.E.; Maksymovych, P.; Yu, P.; Gajek, M.; et al. Conduction at domain walls in oxide multiferroics. *Nat. Mater.* **2009**, *8*, 229–234. [[CrossRef](#)] [[PubMed](#)]
7. Catalan, G.; Seidel, J.; Ramesh, R.; Scott, J.F. Domain wall nanoelectronics. *Rev. Mod. Phys.* **2012**, *84*, 119–156. [[CrossRef](#)]
8. Schilling, A.; Byrne, D.; Catalan, G.; Webber, K.G.; Genenko, Y.A.; Wu, G.S.; Scott, J.F.; Gregg, J.M. Domains in ferroelectric nanodots. *Nano Lett.* **2009**, *9*, 3359–3364. [[CrossRef](#)] [[PubMed](#)]
9. Farokhipoor, S.; Noheda, B. Conduction through 71 degrees Domain Walls in BiFeO₃ Thin Films. *Phys. Rev. Lett.* **2011**, *107*, 127601. [[CrossRef](#)] [[PubMed](#)]
10. Catalan, G.; Janssens, A.; Rispens, G.; Csiszar, S.; Seeck, O.; Rijnders, G.; Blank, D.H.; Noheda, B. Polar domains in lead titanate films under tensile strain. *Phys. Rev. Lett.* **2006**, *96*. [[CrossRef](#)] [[PubMed](#)]
11. Viehland, D.D.; Salje, E.K.H. Domain boundary-dominated systems: Adaptive structures and functional twin boundaries. *Adv. Phys.* **2014**, *63*, 267–326. [[CrossRef](#)]
12. Wang, D.W.; Salje, E.K.H.; Mi, S.B.; Jia, C.; Bellaiche, L. Multidomains made of different structural phases in multiferroic BiFeO₃: A first-principles-based study. *Phys. Rev. B* **2013**, *88*, 134107. [[CrossRef](#)]
13. Scott, J.F.; Salje, E.K.H.; Carpenter, M.A. Domain Wall Damping and Elastic Softening in SrTiO₃: Evidence for Polar Twin Walls. *Phys. Rev. Lett.* **2012**, *109*. [[CrossRef](#)] [[PubMed](#)]
14. Salje, E.K.H.; Safarik, D.J.; Modic, K.A.; Gubernatis, J.E.; Cooley, J.C.; Taylor, R.D.; Mihaila, B.; Saxena, A.; Lookman, T.; Smith, J.L.; et al. Tin telluride: A weakly co-elastic metal. *Phys. Rev. B* **2010**, *82*. [[CrossRef](#)]
15. Seidel, J.; Maksymovych, P.; Batra, Y.; Katan, A.; Yang, S.Y.; He, Q.; Baddorf, A.P.; Kalinin, S.V.; Yang, C.H.; Yang, J.C.; et al. Domain Wall Conductivity in La-Doped BiFeO₃. *Phys. Rev. Lett.* **2010**, *105*. [[CrossRef](#)] [[PubMed](#)]
16. Aird, A.; Salje, E.K.H. Sheet superconductivity in twin walls: Experimental evidence of WO_{3-x}. *J. Phys. Condens. Matter* **1998**, *10*, L377–L380. [[CrossRef](#)]
17. Van Aert, S.; Turner, S.; Delville, R.; Schryvers, D.; Van Tendeloo, G.; Salje, E.K. Direct Observation of ferrielectricity at ferroelastic domain boundaries in CaTiO₃ by electron microscopy. *Adv. Mater.* **2012**, *24*, 523–527. [[CrossRef](#)] [[PubMed](#)]
18. Zykova-Timan, T.; Salje, E.K.H. Highly mobile vortex structures inside polar twin boundaries in SrTiO₃. *Appl. Phys. Lett.* **2014**, *104*. [[CrossRef](#)]
19. Yokota, H.; Usami, H.; Haumont, R.; Hicher, P.; Kaneshiro, J.; Salje, E.K.H.; Uesu, Y. Direct evidence of polar nature of ferroelastic twin boundaries in CaTiO₃ obtained by second harmonic generation microscope. *Phys. Rev. B* **2014**, *89*. [[CrossRef](#)]
20. Goncalves-Ferreira, L.; Redfern, S.A.; Artacho, E.; Salje, E.K. Ferrielectric twin walls in CaTiO₃. *Phys. Rev. Lett.* **2008**, *101*. [[CrossRef](#)] [[PubMed](#)]
21. Salje, E.K.H.; Aktas, O.; Carpenter, M.A.; Laguta, V.V.; Scott, J.F. Domains within Domains and Walls within Walls: Evidence for Polar Domains in Cryogenic SrTiO₃. *Phys. Rev. Lett.* **2013**, *111*. [[CrossRef](#)] [[PubMed](#)]

22. Salje, E.K.H.; Scott, J.F. Ferroelectric Bloch-line switching: A paradigm for memory devices. *Appl. Phys. Lett.* **2014**, *105*. [[CrossRef](#)]
23. Bratkovsky, A.M.; Marais, S.C.; Heine, V.; Salje, E.K.H. The theory of fluctuations and texture embryos in structural phase transitions mediated by strain. *J. Phys. Condens. Matter* **1994**, *6*, 3679–3696. [[CrossRef](#)]
24. Parlinski, K.; Heine, V.; Salje, E.K.H. Origin of tweed texture in the simulation of a cuprate superconductor. *J. Phys. Condens. Matter* **1999**, *5*, 497–518. [[CrossRef](#)]
25. Aktas, O.; Salje, E.K.H.; Crossley, S.; Lampronti, G.I.; Whatmore, R.W.; Mathur, N.D.; Carpenter, M.A. Ferroelectric precursor behavior in $\text{PbSc}_{0.5}\text{Ta}_{0.5}\text{O}_3$ detected by field-induced resonant piezoelectric spectroscopy. *Phys. Rev. B* **2013**, *88*. [[CrossRef](#)]
26. Salje, E.K.H. Tweed, twins, and holes. *Am. Mineral.* **2015**, *100*, 343–351. [[CrossRef](#)]
27. Aktas, O.; Carpenter, M.A.; Salje, E.K.H. Polar precursor ordering in BaTiO_3 detected by resonant piezoelectric spectroscopy. *Appl. Phys. Lett.* **2013**, *103*, 2011–2015. [[CrossRef](#)]
28. Kartha, S.; Krumhansl, J.A.; Sethna, J.P.; Wickham, L.K. Disorder-driven pretransitional tweed pattern in martensitic transformations. *Phys. Rev. B* **1995**, *52*, 803–822. [[CrossRef](#)]
29. Salje, E.K.H.; Ding, X.; Aktas, O. Domain glass. *Phys. Status Solidi* **2014**, *251*, 2061–2066. [[CrossRef](#)]
30. Salje, E.K.H.; Carpenter, M.A. Domain glasses: Twin planes, Bloch lines, and Bloch points. *Phys. Status Solidi* **2015**, *252*, 2639–2648. [[CrossRef](#)]
31. Cross, L.E. *Piezoelectricity*; Springer: Berlin/Heidelberg, Germany, 2008; Volume 114, pp. 131–155.
32. Viehland, D.; Wuttig, M.; Cross, L.E. The glassy behavior of relaxor ferroelectrics. *Ferroelectrics* **1991**, *120*, 71–77. [[CrossRef](#)]
33. Kleemann, W. The relaxor enigma—Charge disorder and random fields in ferroelectrics. *J. Mater. Sci.* **2006**, *41*, 129–136. [[CrossRef](#)]
34. Lloveras, P.; Castán, T.; Planes, A.; Saxena, A. *Disorder and Strain-Induced Complexity in Functional Materials*; Kakeshita, T., Fukuda, T., Saxena, A., Planes, A., Eds.; Springer: Berlin/Heidelberg, Germany, 2012; pp. 227–247.
35. Salje, E.K.H.; Ding, X.; Zhao, Z.; Lookman, T. How to generate high twin densities in nano-ferroics: Thermal quench and low temperature shear. *Appl. Phys. Lett.* **2012**, *100*, 98–101. [[CrossRef](#)]
36. Zubko, P.; Catalan, G.; Tagantsev, A.K. Flexoelectric Effect in Solids. *Annu. Rev. Mater. Res.* **2013**, *43*, 387–421. [[CrossRef](#)]
37. Catalan, G.; Lubk, A.; Vlooswijk, A.H.G.; Snoeck, E.; Magen, C.; Janssens, A.; Rispens, G.; Rijnders, G.; Blank, D.H.A.; Noheda, B. Flexoelectric rotation of polarization in ferroelectric thin films. *Nat. Mater.* **2011**, *10*, 963–967. [[CrossRef](#)] [[PubMed](#)]
38. Conti, S.; Müller, S.; Poliakovsky, A.; Salje, E.K.H. Coupling of order parameters, chirality, and interfacial structures in multiferroic materials. *J. Phys. Condens. Matter* **2011**, *23*. [[CrossRef](#)] [[PubMed](#)]
39. Houchmandzadeh, B.; Lajzerowicz, J.; Salje, E.K.H. Order parameter coupling and chirality of domain-walls. *J. Phys. Condens. Matter* **1991**, *3*, 5163–5169. [[CrossRef](#)]
40. Stengel, M. Flexoelectricity from density-functional perturbation theory. *Phys. Rev. B* **2013**, *88*. [[CrossRef](#)]
41. Salje, E.K.H.; Ding, X.; Zhao, Z.; Lookman, T.; Saxena, A. Thermally activated avalanches: Jamming and the progression of needle domains. *Phys. Rev. B* **2011**, *83*. [[CrossRef](#)]
42. Salje, E.K.; Alexe, M.; Kustov, S.; Weber, M.C.; Schiemer, J.; Nataf, G.F.; Kreisel, J. Direct observation of polar tweed in LaAlO_3 . *Sci. Rep.* **2016**, *6*. [[CrossRef](#)] [[PubMed](#)]
43. Salje, E.K.H. *Phase Transitions in Ferroelastic and Co-Elastic Crystals*; Cambridge University Press: Cambridge, UK, 1993.
44. Bhattacharya, K. *Microstructure of Martensite: Why It Forms and How It Gives Rise to Shape Memory Effects*; Oxford University Press: Oxford, UK, 2004.
45. Sidorkin, A.S. *Domain Structure in Ferroelectrics and Related Materials*; Cambridge International Science Publishing: Cambridge, UK, 2006.
46. Lines, M.; Glass, A. *Principles and Applications of Ferroelectrics and Related Materials*; Clarendon Press: Oxford, UK, 1979.
47. Khachaturyan, A.G. *The Theory of Structural Transformations in Solids*; Wiley: New York, NY, USA, 1983.
48. Scott, J.F. *Ferroelectric Memories*; Springer: Berlin, Germany, 2000.
49. Rabe, K.M.; Triscone, J.M.; Ahn, C.H. *Physics of Ferroelectrics: A Modern Perspective*; Springer: Berlin, Germany, 2007.

50. Jiles, D. *Introduction to Magnetism and Magnetic Materials*; Chapman and Hall: London, UK, 1998.
51. Cullity, B.D.; Graham, C.D. *Introduction to Magnetic Materials*, 2nd ed.; Wiley: New York, NY, USA, 2008.
52. Pavarini, E.; Koch, E.; Schollwock, U. (Eds.) *Emergent Phenomena in Correlated Matter*; Forschungszentrum Julich: Julich, Germany, 2013.
53. Dawber, M.; Rabe, K.M.; Scott, J.F. Physics of thin-film ferroelectric oxides. *Rev. Mod. Phys.* **2005**, *77*. [[CrossRef](#)]
54. Weiss, P. The variation of ferromagnetism with temperature. *Comptes Rendu* **1906**, *143*, 1136.
55. Eerenstein, W.; Mathur, N.D.; Scott, J.F. Multiferroic and magnetoelectric materials. *Nature* **2006**, *442*, 759–765. [[CrossRef](#)] [[PubMed](#)]
56. Spaldin, N.; Fiebig, M. The renaissance of magnetoelectric multiferroics. *Science* **2005**, *309*, 391–392. [[CrossRef](#)] [[PubMed](#)]
57. Fiebig, M. Revival of the magnetoelectric effect. *J. Phys. D Appl. Phys.* **2005**, *38*, R123–R152. [[CrossRef](#)]
58. Kadomtseva, A.; Popov, Y.; Pyatakov, A.; Vorob'ev, G.; Zvezdin, A.K.; Viehland, D. Phase transitions in multiferroic BiFeO₃ crystals, thin-layers, and ceramics: Enduring potential for a single phase, room-temperature magnetoelectric 'holy grail'. *Phase Transit.* **2006**, *79*. [[CrossRef](#)]
59. Salje, E.K.H. Ferroelastic Materials. *Annu. Rev. Mater. Res.* **2012**, *42*, 265–283. [[CrossRef](#)]
60. Salje, E.K.H. Modulated minerals as potential ferroic materials. *J. Phys. Condens. Matter* **2015**, *27*. [[CrossRef](#)] [[PubMed](#)]
61. Hlinka, J.; Privratska, J.; Ondrejovic, P.; Janovec, V. Symmetry Guide to Ferroaxial Transitions. *Phys. Rev. Lett.* **2016**, *116*. [[CrossRef](#)] [[PubMed](#)]
62. Litvin, D.B.; Janovec, V. Spontaneous Tensor Properties for Multiferroic Phases. *Ferroelectrics* **2014**, *461*, 10–15. [[CrossRef](#)]
63. Janovec, V.; Litvin, D.B. Scanning of magnetic space groups and the analysis of non-magnetic domain walls. *Acta Crystallogr. Sect. A* **2007**, *63*, 407–411. [[CrossRef](#)] [[PubMed](#)]
64. Janovec, V. A symmetry approach to domain structures. *Ferroelectric* **1976**, *12*, 43–53. [[CrossRef](#)]
65. Janovec, V. Symmetry and structure of domain walls. *Ferroelectric* **1981**, *35*, 105–110. [[CrossRef](#)]
66. Daumont, C.J.M.; Mannix, D.; Venkatesan, S.; Rubi, D.; Catalan, G.; Kooi, B.J.; de Hosson, J.T.M.; Noheda, B. Epitaxial TbMnO₃ thin films on SrTiO₃ substrates: A structural study. *J. Phys. Condens. Matter* **2009**, *21*. [[CrossRef](#)] [[PubMed](#)]
67. Yadav, A.K.; Nelson, C.T.; Hsu, S.L.; Hong, Z.; Clarkson, J.D.; Schlepütz, C.M.; Damodaran, A.R.; Shafer, P.; Arenholz, E.; Dedon, L.R.; et al. Observation of polar vortices in oxide superlattices. *Nature* **2016**, *530*, 198–201. [[CrossRef](#)] [[PubMed](#)]
68. Poettker, H.; Salje, E.K.H. Flexoelectricity, incommensurate phases and the Lifshitz point. *J. Phys. Condens. Matter* **2016**, *28*, 075902. [[CrossRef](#)] [[PubMed](#)]
69. Zhao, Z.; Ding, X.; Salje, E.K.H. Flicker vortex structures in multiferroic materials. *Appl. Phys. Lett.* **2014**, *105*. [[CrossRef](#)]
70. Aktas, O.; Carpenter, M.A.; Salje, E.K.H. Elastic softening of leucite and the lack of polar domain boundaries. *Am. Mineral.* **2015**, *10*, 2159–2162. [[CrossRef](#)]
71. Aktas, O.; Salje, E.K.H.; Carpenter, M.A. Resonant ultrasonic spectroscopy and resonant piezoelectric spectroscopy in ferroelastic lead phosphate, Pb₃(PO₄)₂. *J. Phys. Condens. Matter* **2013**, *25*. [[CrossRef](#)] [[PubMed](#)]
72. Dove, M.T.; Cool, T.; Palmer, D.C.; Putnis, A.; Salje, E.K.H.; Winkler, B. On the role of Al-Si ordering in the cubic-tetragonal phase transition of leucite. *Am. Mineral.* **1993**, *78*, 486–492.
73. Salje, E. Thermodynamics of plagioclases I: Theory of the I1⁻–P1⁻ phase transition in anorthite and Ca-rich plagioclases. *Phys. Chem. Miner.* **1987**, *14*, 181–188. [[CrossRef](#)]
74. Salje, E.K.H.; Wruck, B. Specific-heat measurements and critical exponents of the ferroelastic phase transition in Pb₃(PO₄)₂ and Pb₃(P_{1-x}As_xO₄)₂. *Phys. Rev. B* **1983**, *28*, 6510–6518. [[CrossRef](#)]
75. Salje, E.; Devarajan, V.; Bismayer, U.; Guimaraes, D.M.C. Phase transitions in Pb₃(P_{1-x}As_xO₄)₂: Influence of the central peak and flip mode on the Raman scattering of hard modes. *J. Phys. C Solid State Phys.* **1983**, *16*, 5233–5243. [[CrossRef](#)]
76. Calleja, M.; Dove, M.T.; Salje, E.K.H. Trapping of oxygen vacancies on twin walls of CaTiO₃: A computer simulation study. *J. Phys. Condens. Matter* **2003**, *15*, 2301–2307. [[CrossRef](#)]

77. Goncalves-Ferreira, L.; Redfern, S.A.T.; Artacho, E.; Salje, E.K.H.; Lee, W.T. Trapping of oxygen vacancies in the twin walls of perovskite. *Phys. Rev. B* **2010**, *81*. [[CrossRef](#)]
78. Lee, W.T.; Salje, E.K.H.; Goncalves-Ferreira, L.; Daraktchiev, M.; Bismayer, U. Intrinsic activation energy for twin-wall motion in the ferroelastic perovskite CaTiO₃. *Phys. Rev. B* **2006**, *73*, 214110. [[CrossRef](#)]
79. Lee, W.T.; Salje, E.K.H.; Bismayer, U. Influence of point defects on the distribution of twin wall widths. *Phys. Rev. B* **2005**, *72*. [[CrossRef](#)]
80. Wu, X.F.; Rabe, K.M.; Vanderbilt, D. Interfacial enhancement of ferroelectricity in CaTiO₃/BaTiO₃ superlattices. *Phys. Rev. B* **2011**, *83*. [[CrossRef](#)]
81. Salje, E.K.H.; Aktas, O.; Ding, X. *Functional Topologies in (Multi-) Ferroics: The Ferroelastic Template. Topological Structures in Ferroic Materials*; Springer Series in Materials Science; Springer: Basel, Switzerland, 2016; Volume 228, pp. 83–101.
82. Tagantsev, A.K.; Courtens, E.; Arzel, L. Prediction of a low-temperature ferroelectric instability in antiphase domain boundaries of strontium titanate. *Phys. Rev. B* **2001**, *64*. [[CrossRef](#)]
83. Kityk, A.V.; Schranz, W.; Sondergeld, P.; Havlik, D.; Salje, E.K.H.; Scott, J.F. Low-frequency superelasticity and nonlinear elastic behavior of SrTiO₃ crystals. *Phys. Rev. B* **2000**, *61*, 946–956. [[CrossRef](#)]
84. Kityk, A.V.; Schranz, W.; Sondergeld, P.; Havlik, D.; Salje, E.K.H.; Scott, J.F. Nonlinear elastic behaviour of SrTiO₃ crystals in the quantum paraelectric regime. *Europhys. Lett.* **2000**, *50*, 41–47. [[CrossRef](#)]
85. Chrosch, J.; Salje, E.K.H. Near-surface domain structures in uniaxially stressed SrTiO₃. *J. Phys. Condens. Matter* **1998**, *10*, 2817–2827. [[CrossRef](#)]
86. Buckley, A.; Rivera, J.P.; Salje, E.K.H. Twin structures in tetragonal SrTiO₃: The ferroelastic phase transition and the formation of needle domains. *J. Appl. Phys.* **1999**, *86*, 1653–1656. [[CrossRef](#)]
87. Salje, E.K.H.; Gallardo, M.C.; Jimenez, J.; Romero, F.J.; del Cerro, J. The cubic-tetragonal phase transition in strontium titanate: Excess specific heat measurements and evidence for a near-tricritical, mean field type transition mechanism. *J. Phys. Condens. Matter* **1998**, *10*, 5535–5543. [[CrossRef](#)]
88. Fontcuberta, J.; Skumryev, V.; Laukhin, V.; Granados, X.; Salje, E.K.H. Polar domain walls trigger magnetoelectric coupling. *Sci. Rep.* **2015**, *5*. [[CrossRef](#)] [[PubMed](#)]
89. Hlinka, J.; Stepkova, V.; Marton, P.; Ondrejovic, P. Ferroelectric Domain Walls and their Intersections in Phase-Field Simulations. In *Topological Structures in Ferroic Materials: Domain Walls, Vortices and Skyrmions*; Springer Series in Materials Science; Springer: Basel, Switzerland, 2016; Volume 228, pp. 161–180.
90. Stepkova, V.; Marton, P.; Hlinka, J. Ising lines: Natural topological defects within ferroelectric Bloch walls. *Phys. Rev. B* **2015**, *92*, 094106. [[CrossRef](#)]
91. Prosandeev, S.; Malashevich, A.; Gui, Z.; Louis, L.; Walter, R.; Souza, I.; Bellaiche, L. Natural optical activity and its control by electric field in electrotoroidic systems. *Phys. Rev. B* **2013**, *87*. [[CrossRef](#)]
92. Conti, S.; Weikard, U. Interaction between free boundaries and domain walls in ferroelastics. *Eur. Phys. J. B* **2004**, *41*, 413–420. [[CrossRef](#)]
93. Salje, E.K.H.; Zhao, Z.; Ding, X.; Sun, J. Mechanical spectroscopy in twinned minerals: Simulation of resonance patterns at high frequencies. *Am. Mineral.* **2013**, *98*, 1449–1458. [[CrossRef](#)]
94. Zhang, L.; Salje, E.K.H.; Ding, X.; Sun, J. Strain rate dependence of twinning avalanches at high speed impact. *Appl. Phys. Lett.* **2014**, *104*. [[CrossRef](#)]
95. Salje, E.K.H.; Wang, X.; Ding, X.; Sun, J. Simulating acoustic emission: The noise of collapsing domains. *Phys. Rev. B* **2014**, *90*. [[CrossRef](#)]
96. Tybell, T.; Paruch, P.; Giamarchi, T.; Triscone, J.M. Domain Wall Creep in Epitaxial Ferroelectric Pb(Zr_{0.2}Ti_{0.8})O₃ Thin Films. *Phys. Rev. Lett.* **2002**, *89*. [[CrossRef](#)] [[PubMed](#)]
97. Chang, L.W.; Nagarajan, V.; Scott, J.F.; Gregg, J.M. Self-Similar Nested Flux Closure Structures in a Tetragonal Ferroelectric. *Nano Lett.* **2013**, *13*, 2553–2557. [[CrossRef](#)] [[PubMed](#)]
98. Salje, E.K.H.; Li, S.; Stengel, M.; Gumbsch, P.; Ding, X. Flexo-electricity and the polarity of complex ferroelastic twin patterns. *Phys. Rev. B* **2016**, *94*. [[CrossRef](#)]
99. Hayward, S.A.; Morrison, F.D.; Redfern, S.A.T.; Salje, E.K.H.; Scott, J.F.; Knight, K.S.; Tarantino, S.C.; Glazer, A.M.; Shuvaeva, V.; Daniel, P.; et al. Transformation processes in LaAlO₃: Neutron diffraction, dielectric, thermal, optical, and Raman studies. *Phys. Rev. B* **2005**, *72*. [[CrossRef](#)]
100. Garten, L.M.; Trolier-McKinstry, S. Enhanced flexoelectricity through residual ferroelectricity in barium strontium titanate. *J. Appl. Phys.* **2015**, *117*. [[CrossRef](#)]

101. Biancoli, A.; Fancher, C.M.; Jones, J.L.; Damjanovic, D. Breaking of macroscopic centric symmetry in paraelectric phases of ferroelectric materials and implications for flexoelectricity. *Nat. Mater.* **2015**, *14*, 224–229. [[CrossRef](#)] [[PubMed](#)]
102. Parkin, S.; Yang, S.H. Memory on the racetrack. *Nat. Nanotechnol.* **2015**, *10*, 195–198. [[CrossRef](#)] [[PubMed](#)]



© 2016 by the authors; licensee MDPI, Basel, Switzerland. This article is an open access article distributed under the terms and conditions of the Creative Commons Attribution (CC-BY) license (<http://creativecommons.org/licenses/by/4.0/>).